Characterization of Two- and Three-Phase Relative Permeability of Water-Wet Porous Media through X-Ray Saturation Measurements

Leili Moghadasi[(1)*], Alberto Guadagnini[(2, 3)], Fabio Inzoli[(1)], Martin Bartosek[(4)], Dario Renna[(4)]

[(1)] Department of Energy, Politecnico di Milano, Via Lambruschini 4, 20156 Milano, Italy

[(2)] Department of Civil and Environmental Engineering, Politecnico di Milano, Piazza Leonardo da Vinci 32, 20133 Milano, Italy

[(3)] Department of Hydrology and Water Resources, The University of Arizona, Tucson, AZ, 85721, USA

[(4)] Eni-Upstream and Technical Services, Petroleum Engineering Laboratories, 20097 Milano, Italy.

* Corresponding author. Tel. +39 02 2399 3826. Fax. +39 02 2399 3913;

E-mail address: leili.moghadasi@polimi.it

Abstract

We present experimental investigations of multi-phase (two-phase (oil/water, oil/gas) and three-phase (oil/ water/ gas)) relative permeabilities performed on laboratory scale rock cores. Two- and three-phase relative permeabilities data were obtained on two core samples (a Sand-pack and a Berea sandstone) by way of a Steady-State (SS) technique. Spatial and temporal dynamics of in-situ saturations along core samples were directly measured through an X-Ray absorption technology. The latter rendered detailed distributions of (section-averaged) fluid flow phases through the medium, which can then be employed for the characterization of relative permeabilities. The technique also enabled us to clearly identify the occurrence of end-effects during the experiments and to quantify the reliability of corrective strategies. For the oil/water settings we considered low and high viscose oil, our findings supporting the observation that relative permeability to oil and water was sensitive to oil viscosity. Three-phase experiments were performed by following an IDI (Imbibition-Drainage-Imbibition) saturation path. The complete experimental data-base is here illustrated and juxtaposed to results obtained by the implementation of simple and commonly employed three-phase relative permeability models. In the three-phase setting, water and gas relative permeabilities display an approximately linear dependence on the logarithm of their own saturation. Consistent with the observation that oil behaves as an intermediate phase in our system, three-phase oil relative permeabilities lie in between those of their two-phase counterparts. Our data-set stands as a reliable reference for further model development and testing, as only a limited quantity of three-phase data are currently available.

Keywords: Two-phase relative permeability, Three-phase relative permeability, Steady-State (SS) technique, X-Ray absorption technology, Three-phase relative permeability models.

Highlights:

- We perform Steady-State (SS) two- and three-phase relative permeability measurements.
- We illustrate the applicability of X-Ray techniques to obtain detailed in-situ measurements of spatial distributions of fluid saturations.
- We investigate the effect of oil/water viscosity ratio on relative permeability curves.
- We probe the performance of a set of simple three-phase relative permeability models against our experimental data.

1. INTRODUCTION

Quantification of multi-phase flow processes taking place in natural porous and fractured rocks has a remarkable relevance to economically sustainable management and viable development of oil- and gas-bearing geologic formations. Characterization of multi-phase flow phenomena is associated with a level of complexity which is considerably higher than that related to the assessment of subsurface systems where single-phase flows take place, because of the need to properly consider the joint (and nonlinear) effects of several factors, including, e.g., interfacial tension, rock wettability and pore size distribution. Attributes of reservoir rocks governing the migration and storage of fluids are key parameters, and their reliable characterization is required for effective reservoir engineering applications. In this context, simultaneous flow of two- and three- fluid phases (i.e., oil, water and gas) in porous media is typically grounded on a continuum- (or Darcy-) scale description which imbues relative permeabilities as key system attributes/parameters to be estimated and linked to state variables, such as fluid saturations. Estimates of the spatial distribution of relative permeabilities are then employed to guide quantification of productivity, injectivity, and ultimate recovery from reservoirs in the context of evaluation and planning of production operations. Relative permeability information can also be used to diagnose the occurrence of formation damage under diverse operational conditions.

Laboratory-scale experiments of two- and three-phase flow are at the core of the characterization of relative permeabilities of diverse rock types, as a function of the flowing fluid types and reservoir conditions. These experiments are generally performed under Steady-State (SS) or Unsteady-State (USS) conditions. While one may expect to obtain similar values of permeabilities for a rock-fluid system via either of these techniques, comparative studies have sometimes exhibited some

discrepancies amongst the results (Dehghanpour, 2011; Dehghanpour et al., 2011; Dehghanpour et al., 2010; Kikuchi et al., 2005; Maini et al., 1990). For instance, unsatisfactory estimates of relative permeabilities have been observed under USS conditions, depending on the data interpretation method employed (Hirasaki et al., 1995; Kerig and Watson, 1986; Maini et al., 1990).

In the Steady-State approach, all phases (e.g., water, oil, and gas) are simultaneously injected into a laboratory core of porous medium and a variety of fixed, metered fractional flow rates are considered in a suite of experiments. While SS experiments are more time-consuming and expensive than their USS counterparts, they offer the advantage of simpler data elaboration and more immediate control on the saturation path. Additionally, and depending on the amount of experimental data collected at diverse fluid saturation levels, SS experiments capture the complete dependence of relative permeability on fluid saturation. Otherwise, USS experiments are characterized by a robust control only on the end-points in the saturation space and require the use of a model to estimate the full relative permeability curves.

From an experimental standpoint, the accurate characterization of the spatial distribution of the proportions between volumetric fractions of fluids displacing in a test rock sample is critical, because of the dependence of relative permeability values on fluid saturations. Energy absorption techniques are very often employed to describe qualitatively and quantitatively the real-time evolution of fluid saturations within core plugs during tests (Maloney, 2003; Maloney et al., 1999; Naylor and Puckett, 1994). Amongst the techniques that can be employed, X-Ray scanning is a non-destructive approach for the characterization of pore-scale rock properties and fluid saturation in core samples. Advantages associated with the use of X-Ray scanning technologies for the study of fluid flow within core plugs include: (*a*) the absence of a strict requirement on accurate measurements of fluid volumes during the experiment (i.e., inlet/outlet volumes of fluid injected/produced); (*b*) the absence of influence of fluid emulsion on in-situ saturation measurements (Maloney et al., 2002); (*c*) the possibility of identifying

the effect on fluid saturation of local heterogeneities which are spatially distributed along the test sample (a feature which might be especially relevant in carbonate cores); and (*d*) the possibility of detecting and accurately estimating average core fluid saturations in the presence of end-effects during flooding (Behin et al., 2011; Maloney, 2003; Spinler and Maloney, 2001).

Accurate and robust experimental data on relative permeability for two-phase flow are less challenging to obtain than three-phase relative permeabilities. Three-phase flow experiments to characterize relationships between relative permeability and fluid saturations and system behavior are very delicate to perform, costly, and time-consuming. Due to a combination of these reasons, documentation and availability of three-phase relative permeability experiments are much scarcer than those associated with two-phase systems (e.g., Alizadeh and Piri, 2014a, b). This is in stark contrast with the observation that three-phase relative permeability (experimental and modeling) studies are becoming increasingly essential in field oriented projects. Several three-phase relative permeability models have been proposed (Baker, 1998; Corey et al., 1956; Delshad et al., 1985; Ebeltoft et al., 1998; Ebeltoft, 2013; Jerauld, 1997; Lomeland et al., 2005; Maini et al., 1989; Skauge and Larsen, 1994; Stone, 1970) and there is a dire need of high quality data for detailed comparative studies on their predictive and interpretive skill.

In this context, our main objectives are (*a*) to illustrate the applicability of X-Ray techniques to obtain in-situ measurements of detailed spatial distributions of fluid saturations along laboratory-scale cores as a function of the viscosity ratio of the displacing fluids under two-phase flow conditions taking place in diverse rock types; and (*b*) to employ the X-Ray technique to document the results of two- and three-phase SS flow experiments which are then used to inform modeling of relative permeability curves as a function of average fluid saturations within the core.

The structure of the work is described in the following. Section 2 describes details of the experimental setup, the rock-fluid system, experimental procedure and the way two- and three-phase

saturations are measured and relative permeabilities are modeled. Section 3 illustrates our experimental findings. We start from results of two-phase experiments and highlight the key added value of grounding in-situ saturation measurements on the X-Ray technique, also by considering the effect of employing diverse types of oils, characterized by contrasting viscosities, to characterize oil relative permeabilities in an oil/water system. Three-phase relative permeability data are then illustrated and discussed in light of typically employed simple interpretive models.

2. Materials and Methods

2.1 Fluids and core samples

The porous media we considered are a Sand-pack and a Berea sandstone. Both media are typically water-wet. Each core is 30 cm long and was placed inside a rubber sleeve with inner diameter of 3.81 cm. A confining pressure p_{conf} = 30 bar was applied to stabilize the packing and prevent flow near the edges.

The fluids used in the displacement experiments were water and Nitrogen (N_2), with isoparaffinic mineral oil (Soltrol-130) and a lubricant oil (OB-12), respectively employed as low and high viscose oil in our two-phase experiments. Sodium Bromide (NaBr) and Potassium Bromide (KBr) were added to the water as X-Ray absorbing chemicals, respectively for the experiments performed on the Sand-pack and on the Berea sample. This enabled us to (*a*) monitor depth- (i.e., section-) averaged fluid saturation along the core and (*b*) increase the contrast between the X-Ray absorption characteristics of oil and water. The choice of these two different compounds was related to the need of eliminating the possibility of the occurrence of reactions with the host porous matrix, which could damage the core structure. Table 1 lists the properties of the core sample and fluids employed in the experiments.

Table 1.

2.2 Experimental setup and condition

Fig. 1 depicts a sketch of the experimental setup. It consists of Hassler-type core holders (TEMCO FCH-1.5 m) containing the samples and the X-Ray saturation monitoring instrumentation (Core Lab Instruments), embedded in a closed loop system. The experiments were performed through the SS technique. Saturation measurements were performed via X-Ray saturation monitoring. The X-Ray equipment includes a generator and a detector, a composite carbon core holder and a data acquisition device. The porous medium samples were positioned vertically inside a Hassler-type core holder and subject to the confinement pressure indicated in Section 2.1. All experiments were conducted at a temperature of 25 °C. The rock samples were scanned from bottom to top by employing a 0.2 mm vertical scanning pitch of the X-Ray system (resulting in a number of 150 saturation readings uniformly distributed along the 0.3 m long samples). We set the X-Ray system at the energy level of 55 kV-30 mA for the two-phase experiments, a value which was selected after some preliminary calibrations of the system (not shown). For the three-phase experiments we considered the same vertical resolution as in the two-phase flow. Consistent with standard operational procedures (Dehghanpour et al., 2010; Morgan et al., 1950; Oak, 1988), we operated the X-Ray system at two diverse energy levels, which we set to 55 kV-30 mA (E_1), and 90 kV-1 mA (E_2), following preliminary system calibrations (not shown).

The design of the system as a closed loop allowed for direct volumetric readings and provides an independent check on the quality of the saturations measured through the X-Ray technology. The streams of oil and water eluted from the system were re-injected from the separator (see Fig. 1) into the core by dual piston volumetric pumps (Pharmacia LKB pump P-500). For the three-phase experiments, gas flows through a humidification system and was then injected into the core by a pump (see Fig. 1). The humidification system essentially comprised a cylinder containing the test oil and water at a temperature of about 40 °C higher than room temperature and the procedure was designed to avoid

drying of the core during gas injection. Two pressure transducers were employed to provide continuous measurements of the pressure drop across the core. Experiments were performed by considering a suite of diverse fluid flow rates and attaining saturation equilibrium for each of these.

Fig. 1.

2.3 Experimental procedure for two-phase flow

We performed several sets of two-phase (oil/water and oil/gas) Steady-State relative permeability experiment, each characterized by a given ratio between the flow rates of oil/water and oil/gas, on the two core samples described in Section 2.1. We started by fully saturating the core samples with water. Absolute water permeability was measured by applying a sequence of diverse flow rates (Step *A* in Fig. 2(*a*)). Joint injections of oil and water was performed by progressively increasing the oil and decreasing the water flow rates (corresponding to drainage). Irreducible water saturation (S_{wi}) was then measured and oil permeability $K_{o(Swi)}$ was assessed at these conditions (Step *B* in Fig. 2(*a*)). A collection of experiments, each characterized by joint injection of oil and water was then performed by decreasing the oil while increasing water flow rates (imbibition), a constant total volumetric flow rate being maintained (Steps *C-E* in Fig. 2(*a*)).

Steady-State oil and gas relative permeabilities were assessed through a set of experiments according to which, similar to the oil/water system, joint injections of oil and gas into the core was performed by increasing the gas and decreasing the oil flow rates at irreducible water saturation (S_{wi}). Oil and gas relative permeabilities were then assessed at gas to liquid flow rate ratios ranging from 0 to 1000, consistent with experiments documented in the literature (e.g., Oak, 1990, Oak et al., 1990).

We remark that X-Ray scans provide longitudinal (i.e., section- / depth-average) saturation profiles of fluids along the cores (with vertical resolution of 2 mm, as stated in Section 2.2). For a given fractional flow setting, measurements of pressure drop across the core and depth-averaged saturation

profiles were taken at steady state, i.e., when no appreciable changes of pressure drop and saturation profiles were observed. Attaining equilibrium (i.e., Steady-State) for each of these steps required (approximately) two days in our setting.

2.4 Experimental procedure for three-phase flow

Three-phase Steady-State relative permeability experiments were performed by simultaneous injections of oil, water and gas into the sample. X-Ray measurements of the dry core, fully saturated with the N_2 gas which was then employed in the multiphase flow experiments, were taken before the beginning of the test to calibrate the equipment under conditions corresponding to full gas saturation of the core. Instrument calibration was performed for both X-Ray energy settings employed in the experiments. The SS three-phase experiments were initiated on the core sample at S_{wi}. Simultaneous injections of oil, water and gas was then performed with increasing water and gas injection rates while decreasing oil injection rate (corresponding to a classical IDI, increasing (or Imbibition) water (I), decreasing (or drainage) oil (D) and increasing (or imbibition) gas (I)) saturation history (Fig. 2(*b*)). The injection rate of each fluid phase and the value of the global pressure drop across the sample were recorded when the system attained steady state.

Fig. 2.

2.5 In-situ saturation measurements

Measurements of water and oil saturation in the two-phase systems are based on (Dehghanpour et al., 2011; Maloney, 2003)

$$S_w = \frac{C_o - C_{o/w}}{C_o - C_w}; \qquad S_o = 1 - S_w; \tag{1}$$

in the oil/water experiments, and

$$S_o = \frac{C_g - C_{g/o}}{C_g - C_o}; \qquad S_g = 1 - S_o; \qquad (2)$$

in the experiments associated with gas and oil migration. Here, S_w, S_o and S_g respectively are saturations of water, oil, and gas; C_o, C_w and C_g are the X-Ray attenuation coefficients associated with full sample saturation by oil, water, and gas, respectively; $C_{o/w}$ and $C_{g/o}$ are attenuation coefficients respectively associated with the oil/water and oil/gas system.

As stated in Section 2.2, a dual X-Ray energy (E_1 and E_2) setting was employed to measure fluid saturations in the three-phase experiments. Two energy levels, corresponding to 55 kV (E_1) and 90 kV (E_2), respectively associated with scanning current of 30 mA and 1 mA, were selected in our experiments. The following two equations relating fluid saturations to X-Ray intensities were employed (Maloney, 2003, Qadeer et al., 2002)

$$(C_w)_{E_i} S_w + (C_o)_{E_i} S_o + (C_g)_{E_i} S_g = (C_{wog})_{E_i} \qquad i = 1, 2 \qquad (3)$$

Here, $(C_w)_{E_1}$, $(C_o)_{E_i}$, and $(C_g)_{E_i}$ are X-Ray intensities respectively corresponding to full sample saturation by oil, water, and gas at 55 kV (for i = 1) or 90 kV (for i = 2), $(C_{wog})_{E_1}$ and $(C_{wog})_{E_2}$ respectively being the intensities at 55 kV and 90 kV under simultaneous flow of the three phases in the system. Saturation values can then be readily calculated by considering that $S_w + S_o + S_g = 1$ (see Appendix A for details).

2.5 Relative permeability estimates

We applied the SS approach to assess relative permeabilities. Capillary equilibrium prevails under these conditions, and permeability values were estimated on the bases of Darcy's law, through quantification of the pressure gradient acting on the phases and the individual phase flow rates. We measured pressure drop across the sample and fluid saturations when the system reached steady state. Effective (absolute) permeabilities under three-phase flow were then estimated as

$$K_o = \frac{q_o \mu_o l}{A \Delta p_o} \; ; \qquad K_w = \frac{q_w \mu_w l}{A \Delta p_w} \; ; \qquad K_g = \frac{2 Q_{N2} p_{atm} \mu_g l}{A (p_{in}^2 - p_{out}^2)} \tag{4}$$

Here, K_o [L^2], K_w [L^2] and K_g [L^2] are absolute oil, water and gas permeability, respectively; q_o and q_w are volumetric flow rates [L^3 T^{-1}] of oil and water, respectively, Q_{N2} [L^3 T^{-1}] volumetric flow rate of gas at the outlet of the sample, which we measured at atmospheric pressure p_{atm} [M L^{-1} T^{-2}]; μ_o, μ_w and μ_g [M L^{-1} T^{-1}] respectively are dynamic viscosity of oil, water and gas; A [L^2] and l [L] are cross-sectional area and sample length; p_{in} and p_{out} [M L^{-1} T^{-2}] respectively are pressure values monitored at the inlet and outlet of the core; $\Delta p_o = \Delta p_w = \Delta p_{core} = p_{in} - p_{out}$ [M L^{-1} T^{-2}] is the global pressure drop between the inlet and outlet of the core. Note that the third of (4) is obtained by (*a*) assuming an ideal gas behavior at the (low) pressure values employed in our experiments and (*b*) expressing Darcy's law in terms of an average/bulk gas flow rate displaced under the action of the average pressure in the core, i.e., (p_{in} + p_{out}) / 2 (Tarek, 2009).

Relative permeabilities (K_{ro}, K_{rw} and K_{rg} respectively for oil, water and gas) are here expressed with respect to oil permeability at irreducible water saturation, $K_{o(Swi)}$, i.e.,

$$K_{ro} = \frac{K_o}{K_{o(Swi)}} \; ; \qquad K_{rw} = \frac{K_w}{K_{o(Swi)}} \; ; \qquad K_{rg} = \frac{K_g}{K_{o(Swi)}} \tag{5}$$

2.6 Three-phase relative permeability models

Several empirical formulations are available to provide predictions/estimates of three-phase oil relative permeability (K_{ro}) as a function of oil relative permeability (and/or fluid saturations) in two-phase settings, i.e., in the presence of water (oil/water system) and in the presence of gas at connate water (oil/gas system). Here, we consider some of the classical and most popular models which are still routinely employed at various stages in the assessment of a reservoir behavior. We purposely selected simple models which allow predicting K_{ro} values solely through two-phase data and three-phase fluid saturations, without the requirement of having at our disposal three-phase relative permeability data,

because a complete comparative analysis of the performance of the wide collection of models available in the literature is outside the scope of this study and is the subject of a future work. A brief recounting of the key features of the models we use is presented in the following.

2.6.1 Corey Model

The following empirical formulation

$$K_{ro} = \frac{(S_L - S_w)^3}{(1 - S_{Lr})^4}(S_w + S_L - 2S_{Lr}) \tag{6}$$

has been proposed by Corey et al. (1956). Here, S_w, S_L and S_{Lr} respectively represent average water saturation, sum of liquid (oil/water) and residual liquid saturations obtained in three-phase experiments.

2.6.2 Stone I Model

Stone (1970) proposed the following empirical model (the so called Stone I model) for three-phase oil relative permeability, K_{ro},

$$K_{ro} = S_o^* \beta_w \beta_g \tag{7}$$

$$\beta_w = \frac{K_{row}}{1 - S_w^*}; \qquad \beta_g = \frac{K_{rog}}{1 - S_g^*} \tag{8}$$

$$S_o^* = \frac{S_o - S_{om}}{1 - S_{wc} - S_{om}}; \qquad S_w^* = \frac{S_w - S_{wc}}{1 - S_{wc} - S_{om}}; \qquad S_g^* = \frac{S_g}{1 - S_{wc} - S_{om}} \tag{9}$$

Here, S_{om} is three-phase residual oil saturation; S_{wc} is connate water saturation; and K_{row} and K_{rog} are two-phase oil relative permeabilities in oil/water and oil/gas systems, respectively. The model is based on channel flow theory and assumes that the maximum value of oil relative permeability in oil/water system is associated with the presence of connate water.

2.6.3 Kokal and Maini Model

Maini et al. (1989) modified the Stone I model as

$$K_{ro} = S_o^* \frac{K_{row}}{K_{row\max}(1-S_w^*)} \frac{K_{rog}}{K_{rog\max}(1-S_g^*)} \frac{K_{row\max}S_w^* + K_{rog\max}S_g^*}{(1-S_o^*)} \quad (10)$$

to allow addressing two main limitations of the Stone I model, associated with the observations that (*a*) data of two-phase oil/gas relative permeability do not always correspond to connate water saturation conditions, and (*b*) experimental values of $K_{row\max}$ and $K_{rog\max}$ are seldom coinciding.

2.6.4 Baker Model

Baker (1998) proposed the following saturation-weighted interpolation model between (two-phase) oil/water and oil/gas data to predict three-phase oil relative permeability

$$K_{ro} = \frac{(S_w - S_{wc})K_{row} + (S_g - S_{gro})K_{rog}}{(S_w - S_{wc}) + (S_g - S_{gro})} \quad (11)$$

where S_{gro} is residual gas saturation in a two-phase (oil/gas) system.

3. RESULTS AND DISCUSSION

Here, we illustrate our experimental results detailing (*a*) the two-phase analyses on two diverse core samples (Sand-pack and Berea sandstone) and (*b*) the three-phase study on the Sand-pack.

3.1 Two-phase experimental results

We mainly focus our illustration of the results of the two-phase experiments on (*a*) the key advantages and benefits associated with the use of the X-Ray technique to measure in-situ fluid saturations along the core and (*b*) the analysis of the influence of the fluid viscosity ratio on the ensuing relative permeability curves expressed as a function of average fluid saturations. Water/oil relative permeability results have been discussed by Moghadasi et al. (2015a, b). A quantitative assessment of experimental uncertainties corresponding to the saturation and permeability data we illustrate is presented in Appendix B.

Relying on direct saturation measurements by the X-Ray in situ saturation monitor obviates for the need of (*a*) employing inlet/outlet tubing volumes and (*b*) measuring fluid levels in the separator,

which are prone to yield additional uncertainties. Fig. 3 provides a graphical depiction of the temporal dynamics of water saturation profiles detected along the Sand-pack core during the drainage process (corresponding to water being displaced by oil). Data in Fig. 3 reveal that significant end effect are detected in the sample at irreducible water saturation S_{wi}. This configuration (dark grey curve in Fig. 3) was attained after 1510 min (corresponding to 89 pore volumes, PV, the estimate of a pore volume being quantified at a pre-test stage through water injection in the dry sample) had elapsed from the beginning of the experiment. End effects are here evidenced by considering that the amount of water saturation detected at sections close to the sample outlet is markedly higher than the actual value detected through X-Ray along the bulk of the core. This observation makes it clear that the absence of in situ saturation measurements could lead to significant overestimation of S_{wi} in water-wet media of the kind we considered. We then eliminated these end effects by further increasing the oil flooding rate at this stage (this procedure being typically referred to as bump flow (Behin et al., 2011; Masalmeh., 2012) until a uniform S_{wi} profile was attained along the sample. Data in Fig. 4 reveal that increasing oil flooding at this later stage (through the above mentioned bump flow) yields an average value of $S_{wi} \approx$ 19%.

Fig. 3.

Fig.4

Corresponding results associated with the Berea sandstone sample are depicted in Fig. 5. Note that end-effects were not observed here because the low permeability of the medium tends to suppress their occurrence.

Fig. 5.

Fig. 6 depicts saturation profiles monitored at Steady-State for the complete set of imbibition experiments performed on the Sand-pack. A fractional flow of water corresponding to 3.12% of the total injection rate was selected as the initial value for this experimental phase, which was associated with joint oil and water joint injection. The X-Ray saturation profiles reveal that there is a significant increase in water saturation even with small water fractional flow. This result is consistent with the water-wet nature of the system and with the observation that the applied oil volumes tend to flow through large pore spaces and most of the pore space has been occupied by water. The saturation profiles and corresponding relative permeability values associated with the oil/gas system flowing in the Sand-pack medium are depicted in Figs. C1 and C2 of Appendix C. These data will be employed in Section 3.3 in conjunction with models illustrated in Section 2.6 to analyze three-phase relative permeabilities.

Fig. 6.

The effect of oil/water viscosity ratio (OWμR) on both oil and water relative permeability curves associated with Berea Sandstone can be detected in Fig. 7. The latter depicts imbibition relative permeability data as a function of water saturation for the oil/water system considering low (LOWμR) and high (HOWμR) oil/water viscosity ratios. These results revealed that both LOWμR permeability curves are shifted towards higher saturation values then their HOWμR counterparts. This evidence is consistent with the observation that using LOWμR yields an increase of connate water saturation and a decrease of residual oil saturation, thus resulting in a facilitated displacement of oil by water. Our results support the conclusions of Torabi et al. (2013), who showed that relative permeability is strongly dependent on OWμR.

Fig. 7.

3.2 Three-phase experimental results

The three-phase tests were performed by following an IDI saturation path in the Sand-pack core, starting at S_{wi}. As stated in Section 3.1, this condition was obtained upon (*a*) achieving full water saturation of the core; and then (*b*) imposing two-phase (oil/water) flow by decreasing the water and increasing the oil saturations to establish S_{wi} (Primary drainage). Simultaneous injection of water, oil and gas were then initiated from this stage (i.e., core at S_{wi}). We started by imposing the largest injection rate for oil while considering the lowest injection rates for water and gas. Each experiment was then performed by considering a progressive increase of water and gas injection rates while decreasing the oil injection rate and keeping a constant liquid (oil/water) injection rate. The end of the sequence of tests corresponds to values of $S_w \approx 61\%$, $S_o \approx 9\%$ and $S_g \approx 30\%$ in the sample.

Fig. 8 depicts the saturation path of our IDI three-phase test. The collection of results of relative permeability to water, oil and gas as a function of the corresponding fluid saturation level are depicted in Fig. C3 of Appendix C. These results reveal that water and gas relative permeabilities display an approximately linear dependence (when plotted in semilogarithmic scale) on their own saturation, a clear nonlinear behavior being associated with oil relative permeability.

Fig. 9 juxtaposes values of water relative permeabilities associated with the experiments performed on the Sand-pack under two- (oil/water) and three-phase conditions as a function of water saturation. In general, there is a good correspondence between the two sets of values. This result is consistent with the observation that water is the wetting phase in the system considered. Following channel flow theory, the wetting phase (i.e., water) tends to occupy the small pores spaces, the non-wetting phase (i.e., gas) being confined in the large pore spaces (with oil separating gas and water). It then follows that water relative permeability in an oil/gas/water system (*a*) is essentially similar to that observed in a water/oil system at a given water saturation, and (*b*) depends solely on water saturation.

A corresponding depiction for gas relative permeabilities as a function of gas saturation is shown in Fig. 10. We note that gas can be considered as a non-wetting phase in our system. Notably, gas relative permeabilities do not appear to display any dependence on the saturation of the remaining two phases.

Fig. 11 depicts the dependence of two- (oil/water and oil/gas) and three-phase oil relative permeabilities on oil saturation. It can be observed that the three-phase oil relative permeabilities, when plotted against oil saturation, are not characterized by a well-defined linear trend when compared against the behavior of water and gas relative permeabilities displayed in Figs. 9 and 10. It is seen that three-phase oil relative permeabilities lie in between those of their two-phase counterparts, their values being mostly close to those of the oil/gas system. These observations are consistent with a phenomenological picture according to which oil, as intermediate phase, tends to occupy the central regions in the pore space. The same type of conclusions are obtained from the IDI-based experimental data sets presented by Oak (1990, 1991), Oak et al. (1990), Skauge and Larsen (1994), Eleri et al. (1995), and Masihi et al. (2011).

Fig. 8.

Fig. 9.

Fig. 10

Fig. 11.

3.3 Interpretation of three-phase experimental data

We probe here the performance of the three-phase relative permeability models illustrated in Section 2.6 to predict our three-phase relative permeability data. We employ the sum of squared deviations

$$\sum DEV = \sum_{i=1}^{N} (K_{ro-lab} - K_{ro-calc})^2. \quad (12)$$

between the experimental ($K_{ro\text{-}lab}$) and model-based values ($K_{ro\text{-}calc}$) of three-phase relative permeabilities as a metric according to which we quantify the skill of each model to represent our experimental data. We remark that the models we selected do not require calibration against three-phase relative permeability data.

As shown in Fig. 12, the model by Baker (11) appears to exhibit sufficient flexibility to adequately reconcile the entire set of experimental data, being associated with the lowest value of (12) (see Table 2). It can be noted that (see also Ahmadloo et al. (2009) and references therein) no single available three-phase predictive model can be considered as a comprehensive tool for accurate prediction of three-phase relative permeabilities. In this context, each of the models we test can introduce significant uncertainties into numerical simulation of multiphase flow in porous media. We further note that all models we considered have been developed on the key premise that three-phase relative permeabilities can be inferred from two-phase data. These modeling assumptions being criticized because they are not always supported by experimental evidences. With reference to the latter point, we emphasize that only a limited quantity of three-phase data are available in the literature (see, e.g., Ahmadloo et al. (2009), Alizadeh and Piri (2014a), Masihi et al. (2011)), so that our data-set can be valuable in assisting for further model development and testing.

Fig. 12.

Table 2.

4. CONCLUSIONS

Our work leads to the following key conclusions.

1. We conducted Steady-State (SS) two-phase oil/water and oil/gas experiments on two porous media samples (a quartz Sand-pack and a Berea sandstone core). Water-, oil- and gas-phase saturations were measured through a X-Ray absorption method. For the oil/water settings we considered low and high viscose oil, our findings supporting the observation that relative permeability to oil and water increase with decreasing oil viscosity. We showed that joint use of our closed loop experimental setup and the X-Ray scanner for direct in situ saturation measurement allowed obtaining high quality data sets. The use of the in-situ X-Ray scanning technology enabled us to (*a*) accurately detect depth-averaged fluid displacement profiles during the flooding, (*b*) identify the occurrence of end-effects and (*c*) quantify the effectiveness of strategies employed to minimize these.
2. We performed Steady-State (SS) three-phase experiments by following an IDI saturation path and provide the complete experimental data-set. We observed that water and gas relative permeabilities display an approximately linear dependence on their own saturation when the latter is subject to a logarithmic transformation, a clear nonlinear behavior being displayed by oil relative permeability. Consistent with the observation that oil behaves as an intermediate phase in our system, three-phase oil relative permeabilities lie in between those of their two-phase counterparts. Otherwise, water relative permeability under three-phase conditions is essentially similar to that observed in a two-phase water/oil system for the medium we analyze.
3. We juxtaposed our experimental data onto results obtained by the implementation of simple and commonly employed three-phase relative permeability models, which are based solely on the use of two-phase relative permeability data. Amongst the models selected, we found that the

model by Baker (11) adequately interprets the entire set of experimental data, model performance being evaluated on the basis of the typical sum of square errors criterion. In this context, our data-set has the added value of providing reliable grounds for further model development and testing, as only a limited quantity of three-phase data are available in the literature.

Appendix A

Three-phase saturation measurements through X-Ray attenuation

X-Ray attenuation due to the combined effect of oil, water, gas and rock matrix can be described through the following

$$(C_w)_{E_1} S_w + (C_o)_{E_1} S_o + (C_g)_{E_1} S_g = (C_{wog})_{E_1} \quad \text{(A1)}$$

$$(C_w)_{E_2} S_w + (C_o)_{E_2} S_o + (C_g)_{E_2} S_g = (C_{wog})_{E_2} \quad \text{(A2)}$$

$$S_w + S_o + S_g = 1 \quad \text{(A3)}$$

Where all symbols are defined in Section 2.5. Substitution of S_w from (A1) into (A2) and (A3) yields

$$(C_w)_{E_1}(1 - S_g - S_o) + (C_o)_{E_1} S_o + (C_g)_{E_1} S_g = (C_{wog})_{E_1} \quad \text{(A4)}$$

$$(C_w)_{E_2}(1 - S_g - S_o) + (C_o)_{E_2} S_o + (C_g)_{E_2} S_g = (C_{wog})_{E_2} \quad \text{(A5)}$$

This leads to

$$S_o = \frac{[(C_{wog})_{E_1} - (C_w)_{E_1}][(C_g)_{E_2} - (C_w)_{E_2}] - [(C_{wog})_{E_2} - (C_w)_{E_2}][(C_{wog})_{E_1} - (C_w)_{E_1}]}{[(C_o)_{E_1} - (C_w)_{E_1}][(C_g)_{E_2} - (C_w)_{E_2}] - [(C_o)_{E_2} - (C_w)_{E_2}][(C_g)_{E_1} - (C_w)_{E_1}]}; \quad \text{(A6)}$$

$$S_g = \frac{[(C_{wog})_{E_1} - (C_w)_{E_1}][(C_o)_{E_2} - (C_w)_{E_2}] - [(C_{wog})_{E_2} - (C_w)_{E_2}][(C_o)_{E_1} - (C_w)_{E_1}]}{[(C_o)_{E_2} - (C_w)_{E_2}][(C_g)_{E_1} - (C_w)_{E_1}] - [(C_o)_{E_1} - (C_w)_{E_1}][(C_g)_{E_2} - (C_w)_{E_2}]}; \quad \text{(A7)}$$

$$S_w = 1 - S_o - S_g \quad \text{(A8)}$$

Appendix B

Quantification of Experimental Uncertainties

We performed our experiments in the closed loop system described in Section 2, to improve our (*a*) ability to control the experimental conditions and (*b*) provide an additional check of saturation measurements obtained through the X-Ray method. Relative differences between core-averaged saturations measured by the two techniques were less than 1% (details not shown).

Calculation of relative permeability relies on direct measurement of the length and diameter of the core, fluid viscosities and injection rates, and the differential pressure across the core. The main sources of uncertainty in this context are related to pressure transducers (measuring pressure across the core) and fluid (oil, water and gas) injection devices (pumps). The uncertainty associated with pressure measurements was ± 2.5 % and it is ± 0.7%, ± 0.7% and ± 1.5%, respectively for the oil, water and gas injection devices, according to the factory specifics of the instrumentation employed. It then follows that uncertainty linked to relative permeability were always less than 1.6% in our experiments.

Appendix C

Experimental results

Here, we collect key experimental results complementing those depicted in Section 3.

Fig. C1.

Fig. C2.

Fig. C3.

TABLE. CAPTIONS

Table 1. Physical properties of the tested core samples and fluids.

Table 2. Values of the sum of squared deviations (12) associated with the oil relative permeability models illustrated in Section 2.6.

FIG. CAPTIONS

Fig. 1. Sketch of the experimental set-up.

Fig. 2. Main steps of the procedure employed for Steady-State (SS) experiments for (a) two- and (b) three-phase settings.

Fig. 3. Temporal dynamics of water saturation profiles detected along the Sand-pack core during the drainage process at diverse observation times (or Pore Volumes, PV) after injection. End effects are clearly visible.

Fig. 4. In-situ irreducible water saturation, S_{wi}, detected along the Sand-pack before and after the application of bump flow to eliminate end effects.

Fig. 5. Temporal dynamics of water saturation profiles detected along the Berea sandstone sample at diverse observation times (or Pore Volumes, PV) after injection during the drainage process (corresponding to water being displaced by oil).

Fig. 6. In-situ saturation profiles monitored at Steady-State (SS) for the complete set of imbibition experiments performed on the Sand-pack.

Fig. 7. Imbibition relative permeability data as a function of water saturation for the oil/water system associated with low (LOWμR) and high (HOWμR) oil/water viscosity ratios.

Fig. 8. Saturation path for the IDI three-phase test on the Sand-pack core.

Fig. 9. Water relative permeabilities associated with the experiments performed on the Sand-pack under two- (oil/water) and three-phase conditions as a function of water saturation.

Fig. 10. Gas relative permeabilities associated with the experiments performed on the Sand-pack under two- (oil/gas) and three-phase conditions as a function of gas saturation.

Fig. 11. Oil relative permeabilities associated with the experiments performed on the Sand-pack under two- (oil water), (oil/gas) and three-phase conditions as a function of oil saturation.

Fig. 12. Comparison between the Steady-State (SS) three-phase oil relative permeability data (K_{ro}) and the corresponding values obtained by applying the models illustrated in Section 2.6.

Fig. C1. In-situ Steady-State (SS) oil saturation profiles detected for the oil/gas system in the Sand-pack medium.

Fig. C2. In-situ Steady-State (SS) oil and gas relative permeabilities (respectively denoted as K_{ro} and K_{rg}) associated with the oil/gas system for the Sand-pack medium.

Fig. C3. Relative permeability to water, oil and gas as a function of the corresponding fluid saturation level.

Conflict of interest

The authors declare that they have no conflict of interest.

Acknolwedgments

Partial financial support from Eni SpA is gratefully acknowledged. AG acknowledges partial funding from the European Union's Horizon 2020 Research and Innovation programme (Project "Furthering the knowledge Base for Reducing the Environmental Footprint of Shale Gas Development" FRACRISK - Grant Agreement No. 636811".

All data are available upon request.

References

Ahmadloo, F., Asghari, K. and Jamaloei, B.Y., 2009. Experimental and Theoretical Studies of Three Phase Relative Permeability. SPE Annual Technical Conference and Exhibition, New Orleans, Louisiana. doi: 10.2118/124538-MS.

Alizadeh, A. H., Piri M., 2014a. Three-phase Flow in Porous Media: A Review of Experimental Studies on Relative Permeability. Rev. Geophys, 52: 468-521. doi: 10.1002/2013RG000433.

Alizadeh, A. H., Piri M., 2014b. The Effect of Saturation History on Three–Phase Relative Permeability: An Experimental Study. Water Resour. Res, 50: 1636-1664. doi: 10.1002/2013WR014914.

Baker, L.E., 1998. Three-Phase Relative Permeability Correlations. SPE Enhanced Oil Recovery Symposium, Tulsa, Oklahoma. doi: 10.2118/17369-MS.

Behin, R., Sharifi Galiuk, H., 2011. Study of Two Phase Fluid Flow in Water Wet Reservoir Rocks by Using X-Ray In situ Saturation Monitoring. Journal of Petroleum Science and Technology, 1(1): 15-23.

Corey, A.T., Rathjens, C.H., Henderson, J.H. and Wyllie, M.R.J., 1956. Three-Phase Relative Permeability. Journal of Petroleum Technology. 8(11): 63-65. doi: 10.2118/737-G.

Dehghanpour, H., 2011. Measurement And Modeling of Three-Phase Oil Relative Permeability. PhD Dissertation. doi: 2152/ETD-UT-2011-12-4700.

Dehghanpour, H., Aminzadeh, B., Mirzaei, M. and DiCarlo, D., 2011. Flow Coupling During Three-Phase Gravity Drainage. Physical Review E. 83(6): 065302. doi: 10.1103/PhysRevE.83.065302.

Dehghanpour, H., DiCarlo, D.A., Aminzadeh, B. and Mirzaei Galeh-Kalaei, M., 2010. Two-Phase and Three-Phase Saturation Routes and Relative Permeability During Fast Drainage. SPE Improved Oil Recovery Symposium, Tulsa, Oklahoma, USA. doi: 10.2118/129962-MS.

Delshad, M., MacAllister, D.J., Pope, G.A. and Rouse, B.A., 1985. Multiphase Dispersion and Relative Permeability Experiments. Society of Petroleum Engineers Journal. 25(4): 524-534. doi: 10.2118/10201-PA.

Ebeltoft, E., Iversen, J., Vatne, K., Andersen, M. and Nordtvedt, J., 1998. A Novel Experimental Ppparatus for Determination of Three-Phase Relative Permeabilities at Reservoir Conditions. Journal of Petroleum Science and Engineering. 19(1): 119-132. doi: 10.1016/S0920-4105(97)00041-7.

Ebeltoft, E., 2013. Versatile Three-Phase Correlations for Relative Permeability and Capillary Pressure. Presented at the International Symposium of the Society of Core Analysts held in Napa Valley, California, USA. SCA 034 (2013): 1-14.

Hirasaki, G., Rohan, J. and Dudley, J., 1995. Interpretation of Oil/Water Relative Permeabilities from Centrifuge Displacement. SPE Advanced Technology Series. 3(01): 66-75. doi: 10.2118/24879-PA.

Jerauld, G., 1997. General Three-Phase Relative Permeability Model for Prudhoe Bay. SPE reservoir Engineering. 12(4): 255-263. doi: 10.2118/36178-PA.

Kerig, P. and Watson, A., 1986. Relative-Permeability Estimation from Displacement Experiments: an Error Analysis. SPE Reservoir Engineering. 1(02): 175-182. doi: 10.2118/12589-PA.

Kikuchi, M.M., Branco, C.C., Bonet, E.J., Zanoni, R.M. and Paiva, C.M., 2005. Water Oil Relative Permeability Comparative Study: Steady Versus UnSteady State. International Symposium of the Society of Core Analysts held in Toronto, Canada. SCA 77 (2005): 1-7.

Lomeland, F., Ebeltoft, E. and Thomas, W.H., 2005. A New Versatile Relative Permeability Correlation. International Symposium of the Society of Core Analysts, Toronto, Canada. SCA 32: 1-12.

Maini, B., Coskuner, G. and Jha, K., 1990. A Comparison of Steady-State and Unsteady-State Relative Permeabilities of Viscocities Oil and Water in Ottawa Sand. Journal of Canadian Petroleum Technology. 29(02). doi: 10.2118/90-02-02.

Maini, B.B., Kokal, S. and Jha, K., 1989. Measurements and Correlations of Three-Phase Relative Permeability at Elevated Temperatures and Pressures. SPE Annual Technical Conference and Exhibition, San Antonio, Texas. doi: 10.2118/19677-MS.

Malavasi, S. and Guadagnini, A., 2003. Hydrodynamic Loading on River Bridges. Journal of Hydraulic Engineering. 129(11): 854-861. doi: 10.1061/(ASCE)0733-9429(2003)129:11(854).

Maloney, D., 2003. X-Ray Imaging Technique Simplifies and Improves Reservoir-Condition Unsteady-State Relative Permeability Measurements. Petrophysics. 44(4): 271-278. doi: SPWLA-2003-v44n4a5.

Maloney, D., Wegener, D. and Zornes, D., 1999. New X-Ray Scanning System for Special Core Analyses in Support of Reservoir Characterization. SCA 9940 (1999): 1-4.

Masalmeh, S., 2012. Impact of Capillary Forces on Residual Oil Saturation and Flooding Experiments for Mixed to Oil-Wet Carbonate Rreservoirs. Presented at the International Symposium of the Society of Core Analysts. SCA 11 (2012).

Masihi, M., Javanbakht, L., Horeh, F.B. and Rasaei, M., 2011. Experimental Investigation and Evaluation of Three-Phase Relative Permeability Models. Journal of Petroleum Science and Engineering. 79(1): 45-53. doi: 10.1016/j.petrol.2011.08.017.

Moghadasi, L., Guadagnini, A., Inzoli, F. and Bartosek, M., 2015a. Interpretation of Two-Phase Relative Permeability Curves through Multiple Formulations and Model Quality Criteria. Journal of Petroleum Science and Engineering. 135: 738-749. doi:10.1016/j.petrol.2015.10.027.

Moghadasi, L., Guadagnini, A., Inzoli, F., Bartosek, M., Colapietro, D., Renna, D., 2015b. Laboratory-Scale Investigation of Two-phase Relative Permeability. Procedia Environmental Sciences. 25: 166-174. doi: 10.1016/j.proenv.2015.04.023.

Morgan, F., McDowell, J.M. and Doty, E.C., 1950. Improvements in the X-Ray Saturation Technique of Studying Fluid Flow. Journal of Petroleum Technology. 2(07): 183-194. doi: 10.2118/950183-G.

Naylor, P. and Puckett, D., 1994. In-Situ Saturation Distributions: the Key to Understanding Core Analysis. Presented at Society of Core Analysts Symposium, Stavanger. SCA 9405 (1994).

Oak, M.J., 1988. A New X-Ray Absorption Method for Measurement of Three-Phase Relative Permeability. SPE Reservoir Engineering, 3(01): 199-206. doi: 10.2118/14420-PA.

Oak, M.J., 1990. Three-Phase Relative Permeability of Water-Wet Berea. Society of Petroleum Engineers. SPE/DOE Enhanced Oil Recovery Symposium,Tulsa, Oklahoma. doi:10.2118/20183-MS.

Oak, M.J., Baker, L.E. and Thomas, D.C., 1990. Three-Phase Relative Permeability of Berea Sandstone. Journal of Petroleum Technology. 42(08). doi:10.2118/17370-PA.

Skauge, A. and Larsen, J.A., 1994. Three-Phase Relative Permeabilities and Trapped Gas Measurements Related to WAG Process. Proceedings of the International Symposium of the Society of Core Analysts, Stavanger, Norway. SCA 21 (1994).

Spinler, E. and Maloney, D., 2001. Application of Linear X-Ray Analysis Using Absorption Coefficients for Direct Determination of In Situ Core Saturation for Pc Measurement, Presented at the SCA Conference, Edinburgh, UK. SCA 31 (2001): 16-19. doi: SCA.1987-2004/1-SCA2001-31.

Stone, H.L., 1970. Probability Model for Estimating Three-Phase Relative Permeability. Journal of Petroleum Technology. 22(02): 214-218. doi: 10.2118/2116-PA.

Tarek, A., 2009. Working Guide to Reservoir Rock Properties and Fluid Flow, Part 2 - Fundamentals of Rock Properties. Gulf Professional Publishing., Boston, pp. 31-115. doi: 10.1016/B978-1-85617-825-9.00002-8.

Highlights:

- We perform Steady-State (SS) two- and three-phase relative permeability measurements.
- We illustrate the applicability of X-Ray techniques to obtain detailed in-situ measurements of spatial distributions of fluid saturations.
- We investigate the effect of oil/water viscosity ratio on relative permeability curves.
- We probe the performance of a set of simple three-phase relative permeability models against our experimental data.

Figure

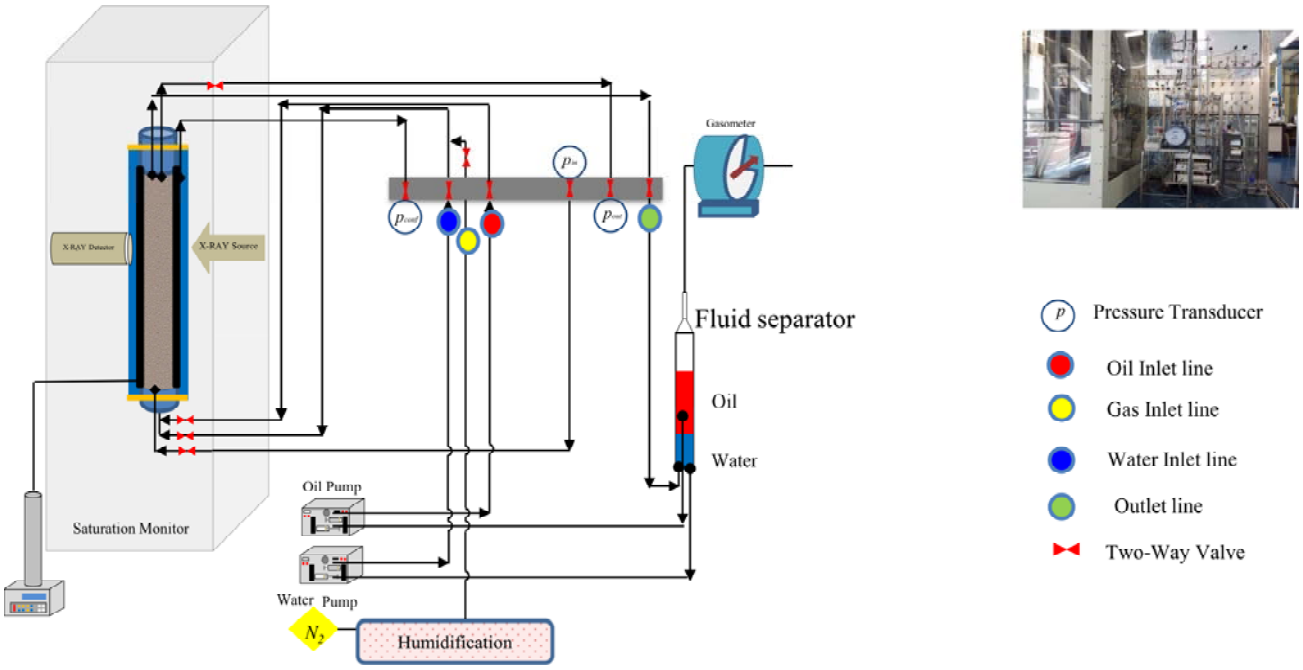

Fig. 1. Sketch of the experimental set-up.

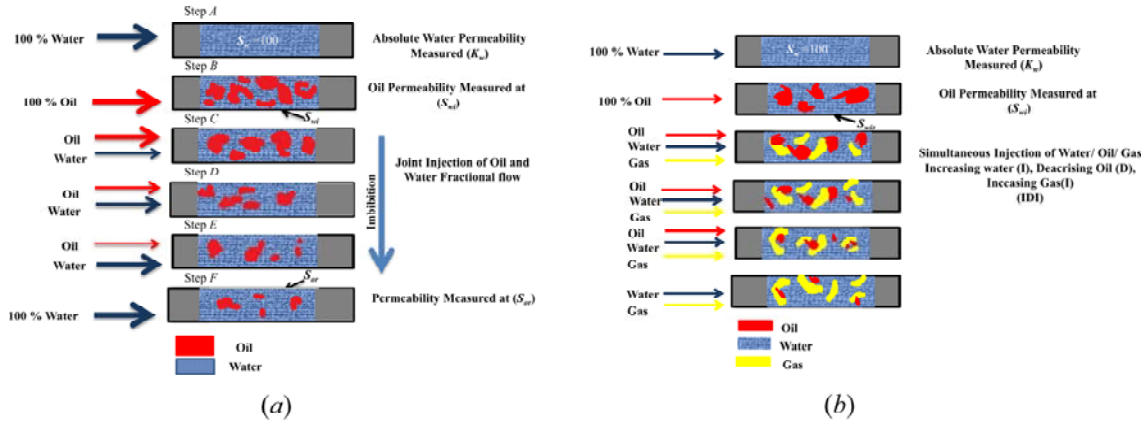

Fig. 2. Main steps of the procedure employed for Steady-State (SS) experiments for (*a*) two- and (*b*) three-phase settings.

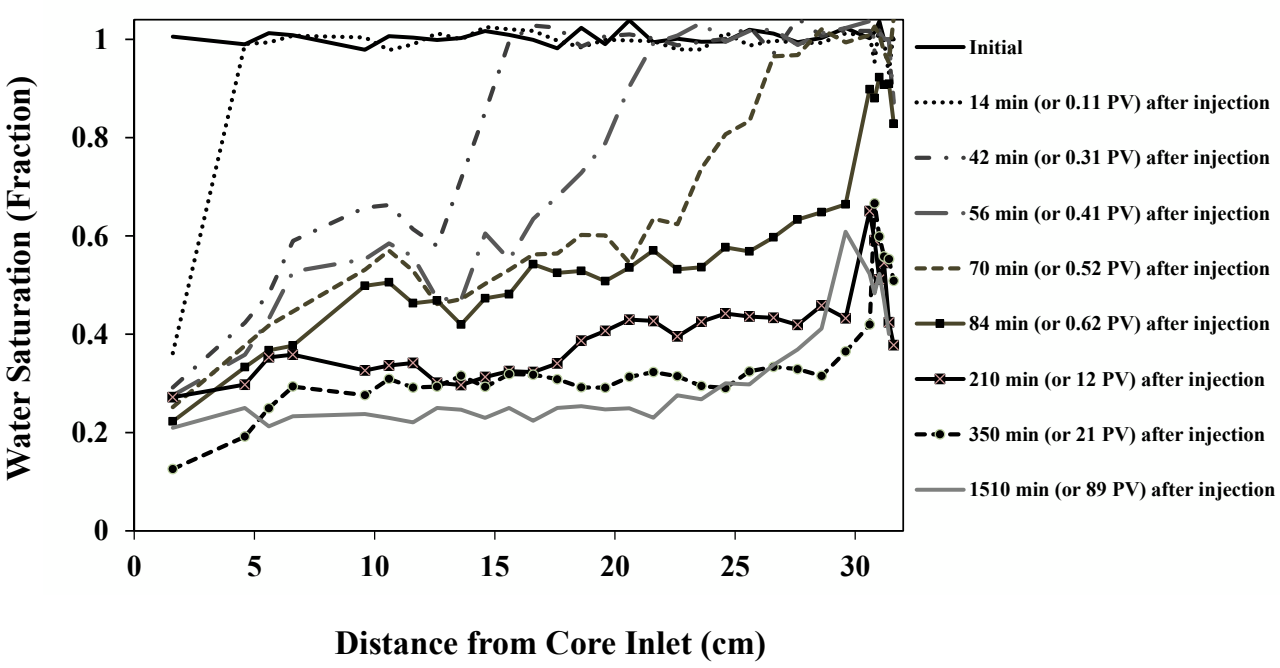

Fig. 3. Temporal dynamics of water saturation profiles detected along the Sand-pack core during the drainage process at diverse observation times (or Pore Volumes, PV) after injection. End effects are clearly visible.

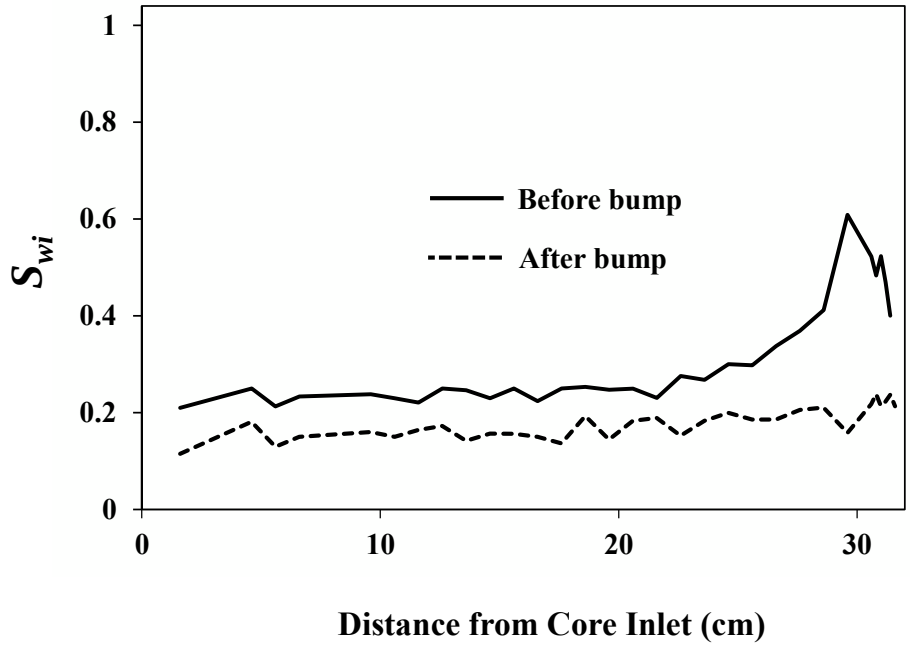

Fig. 4. In-situ irreducible water saturation, S_{wi}, profiles detected along the Sand-pack before and after the application of bump flow to eliminate end effects.

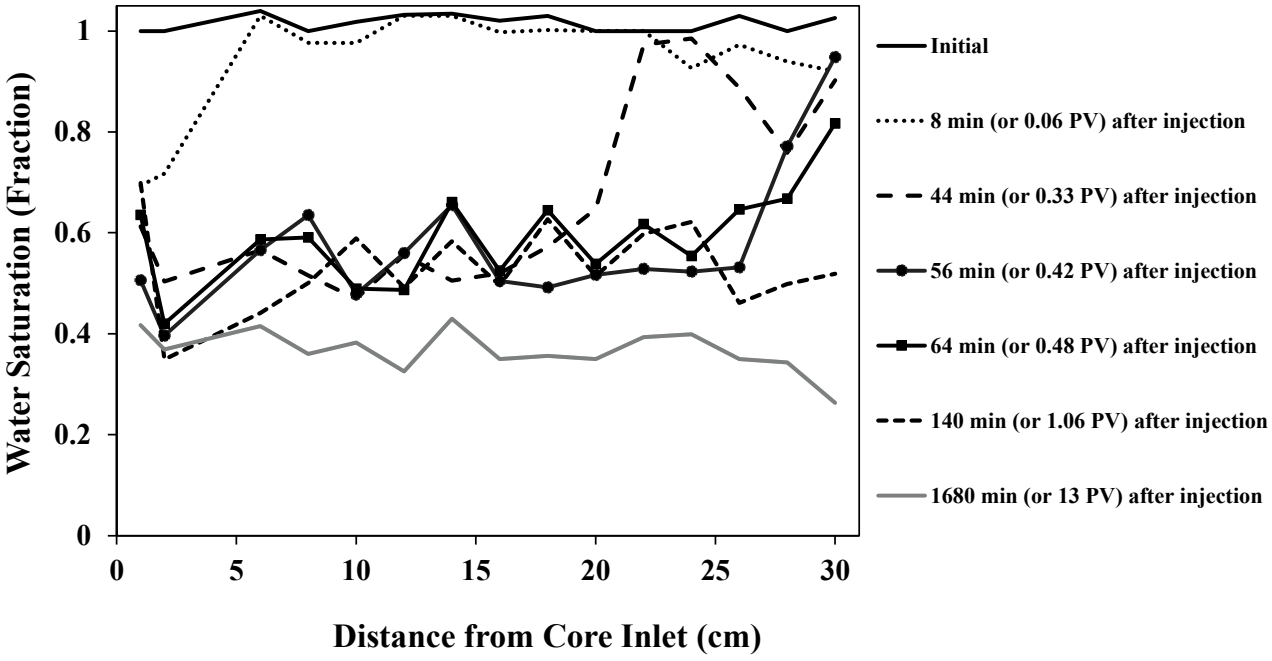

Fig. 5. Temporal dynamics of water saturation profiles detected along the Berea sandstone sample at diverse observation times (or Pore Volumes, PV) after injection during the drainage process (corresponding to water being displaced by oil).

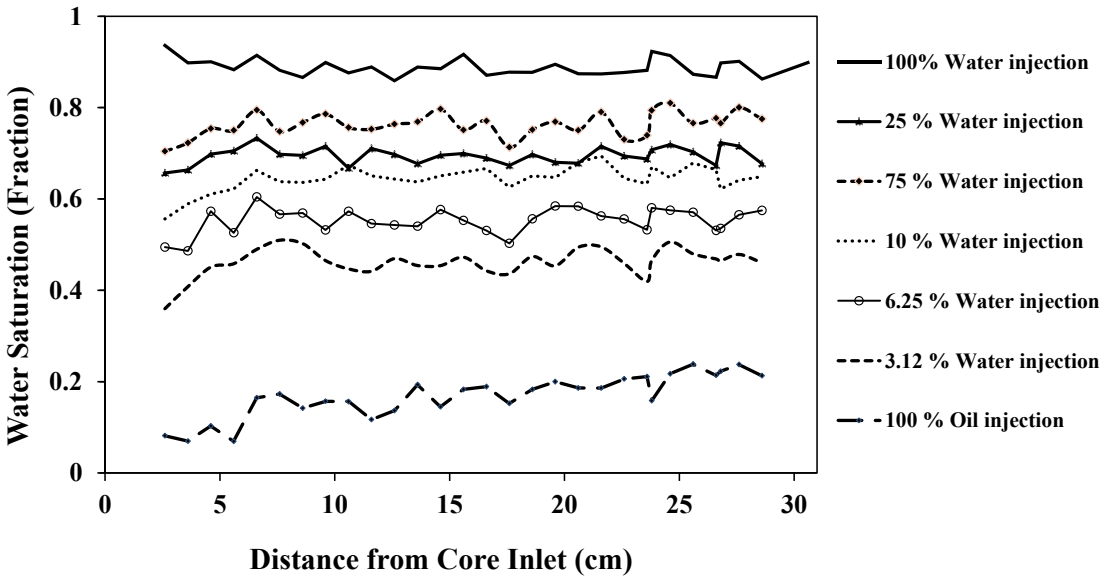

Fig. 6. In-situ saturation profiles monitored at Steady-State (SS) for the complete set of imbibition experiments performed on the Sand-pack.

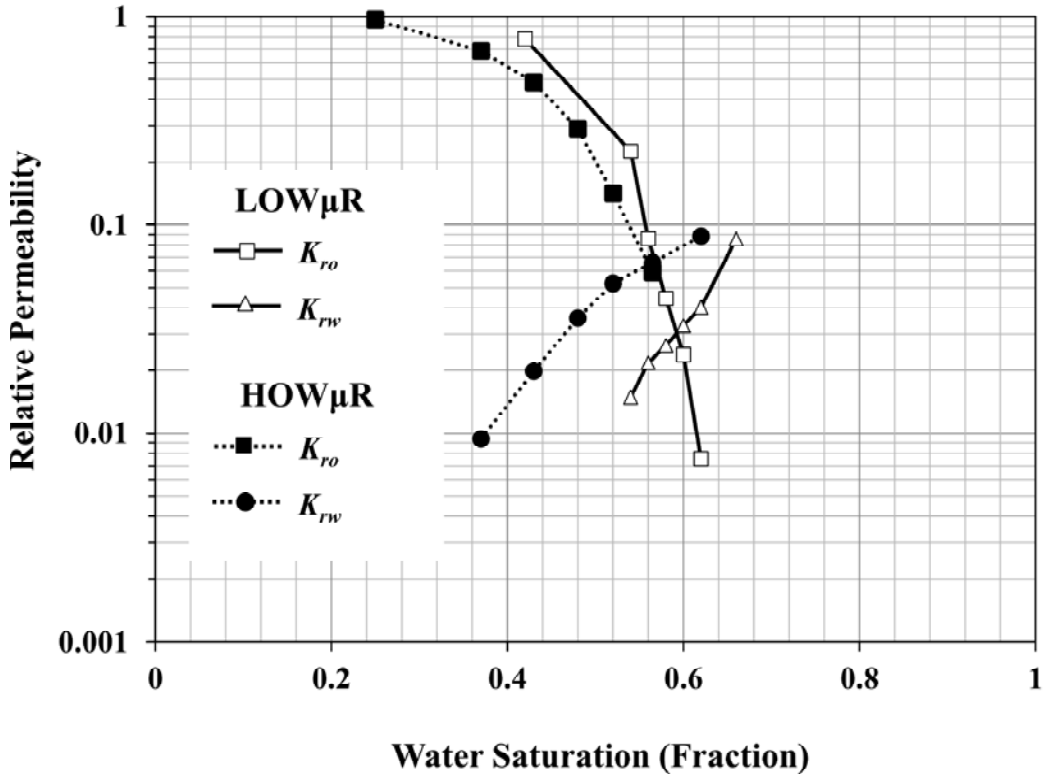

Fig. 7. Imbibition relative permeability data as a function of water saturation for the oil/water system associated with low (LOWμR) and high (HOWμR) oil/water viscosity ratios.

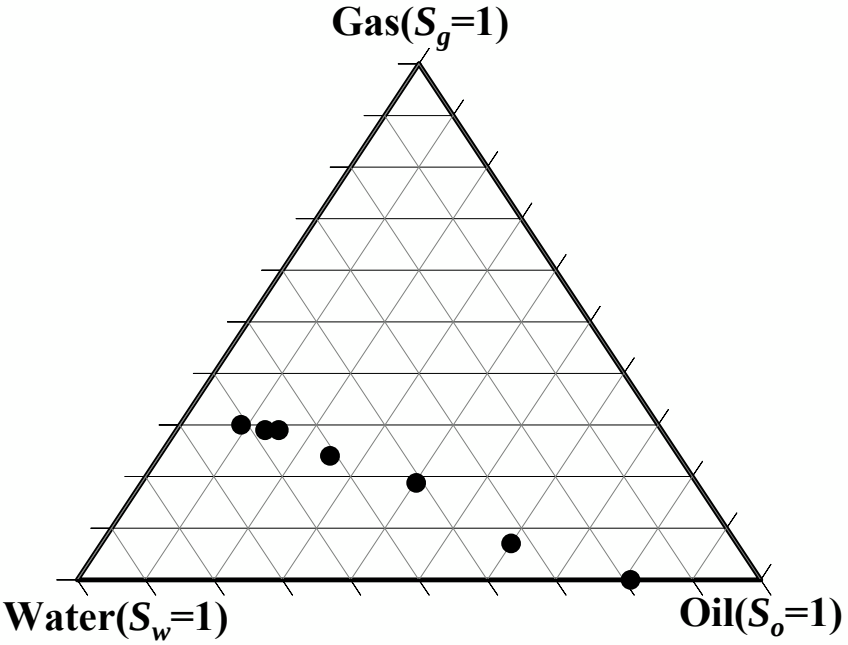

Fig. 8. Saturation path for the IDI three-phase test on the Sand-pack core.

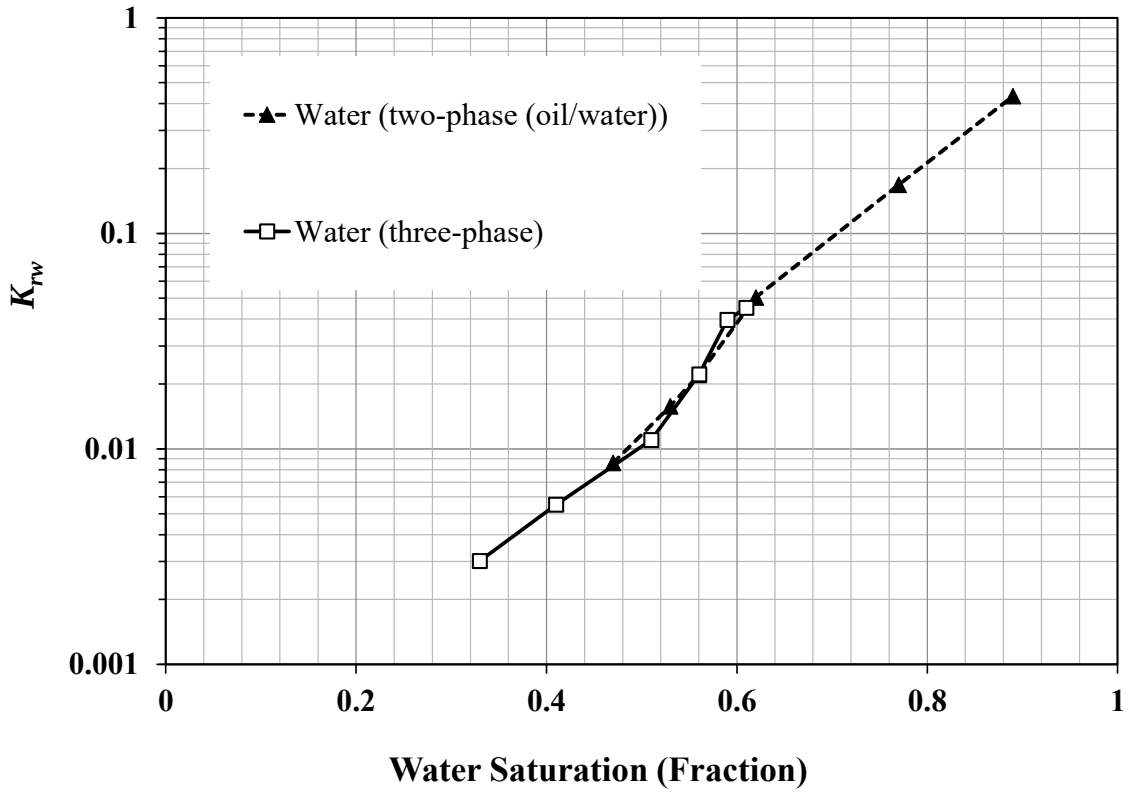

Fig. 9. Water relative permeabilities associated with the experiments performed on the Sand-pack under two- (oil/water) and three-phase conditions as a function of water saturation

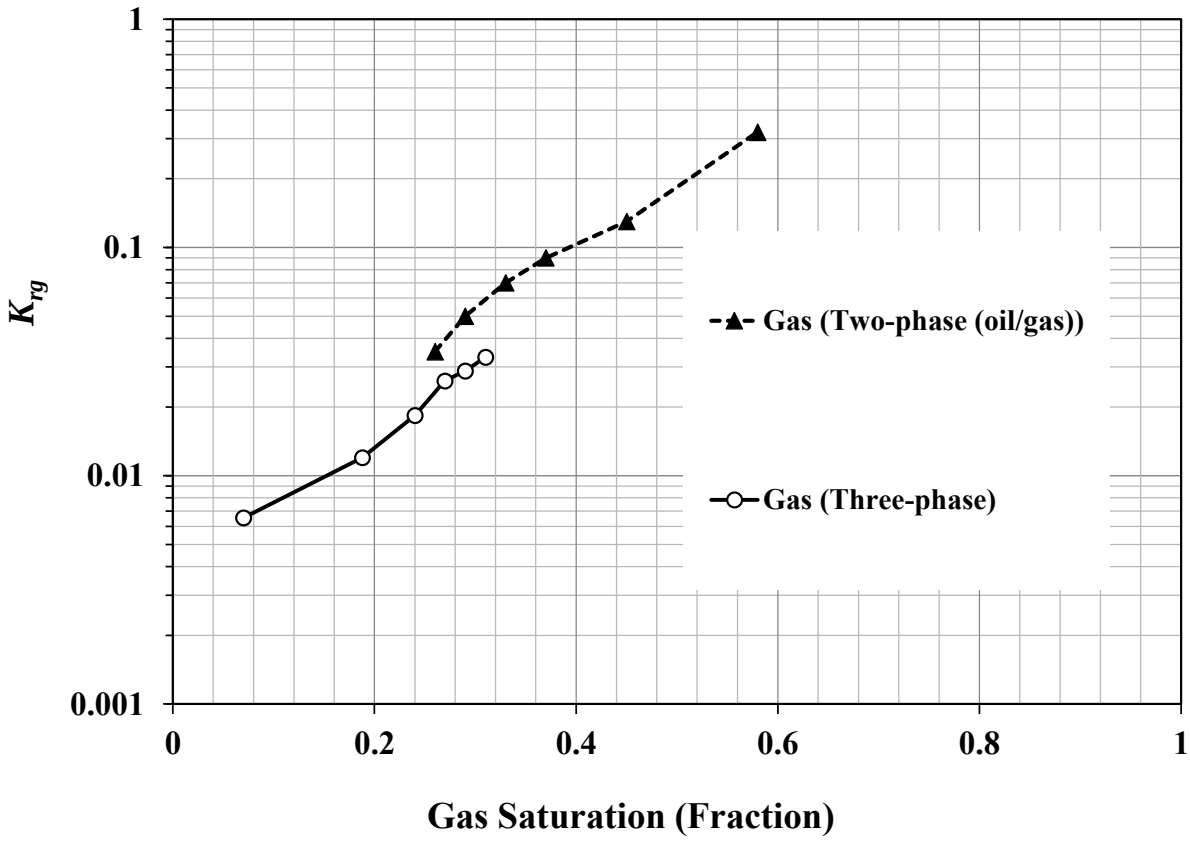

Fig. 10. Gas relative permeabilities associated with the experiments performed on the Sand-pack under two- (oil/gas) and three-phase conditions as a function of gas saturation.

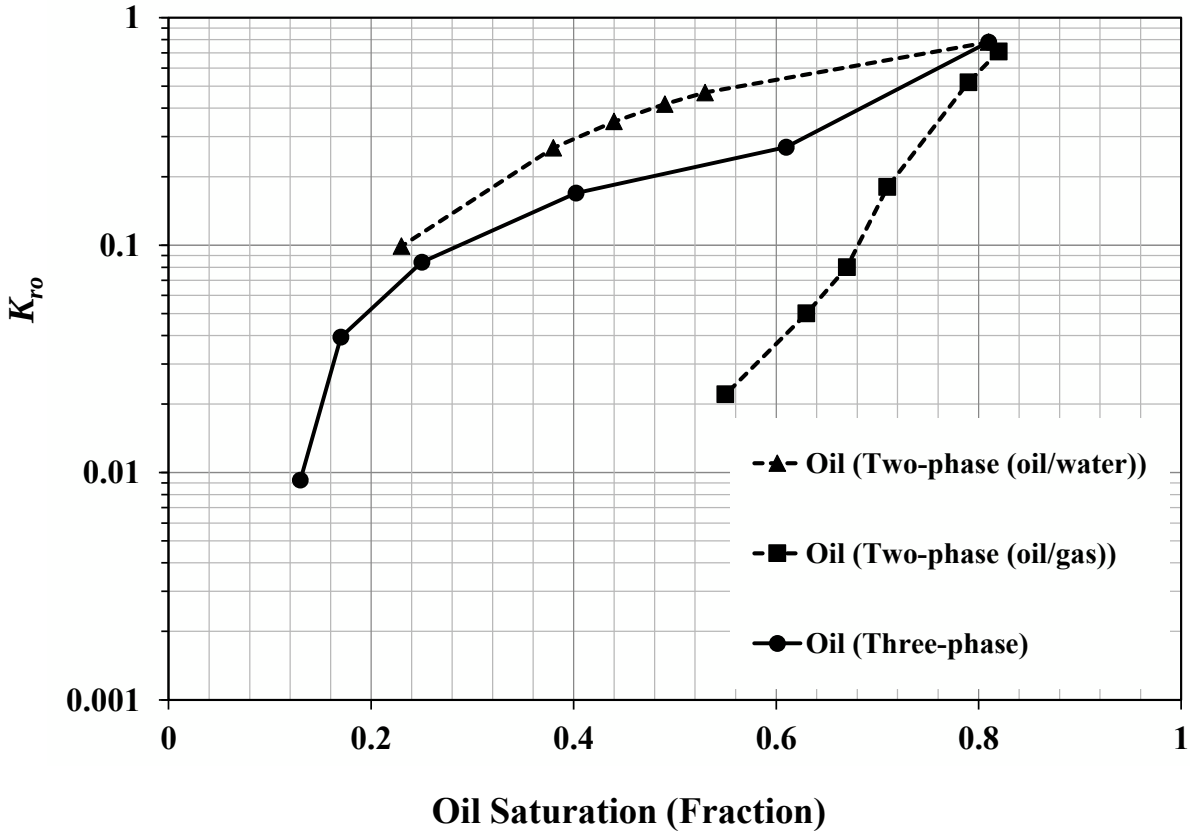

Fig. 11. Oil relative permeabilities associated with the experiments performed on the Sand-pack under two- (oil/water), (oil/gas) and three-phase conditions as a function of oil saturation.

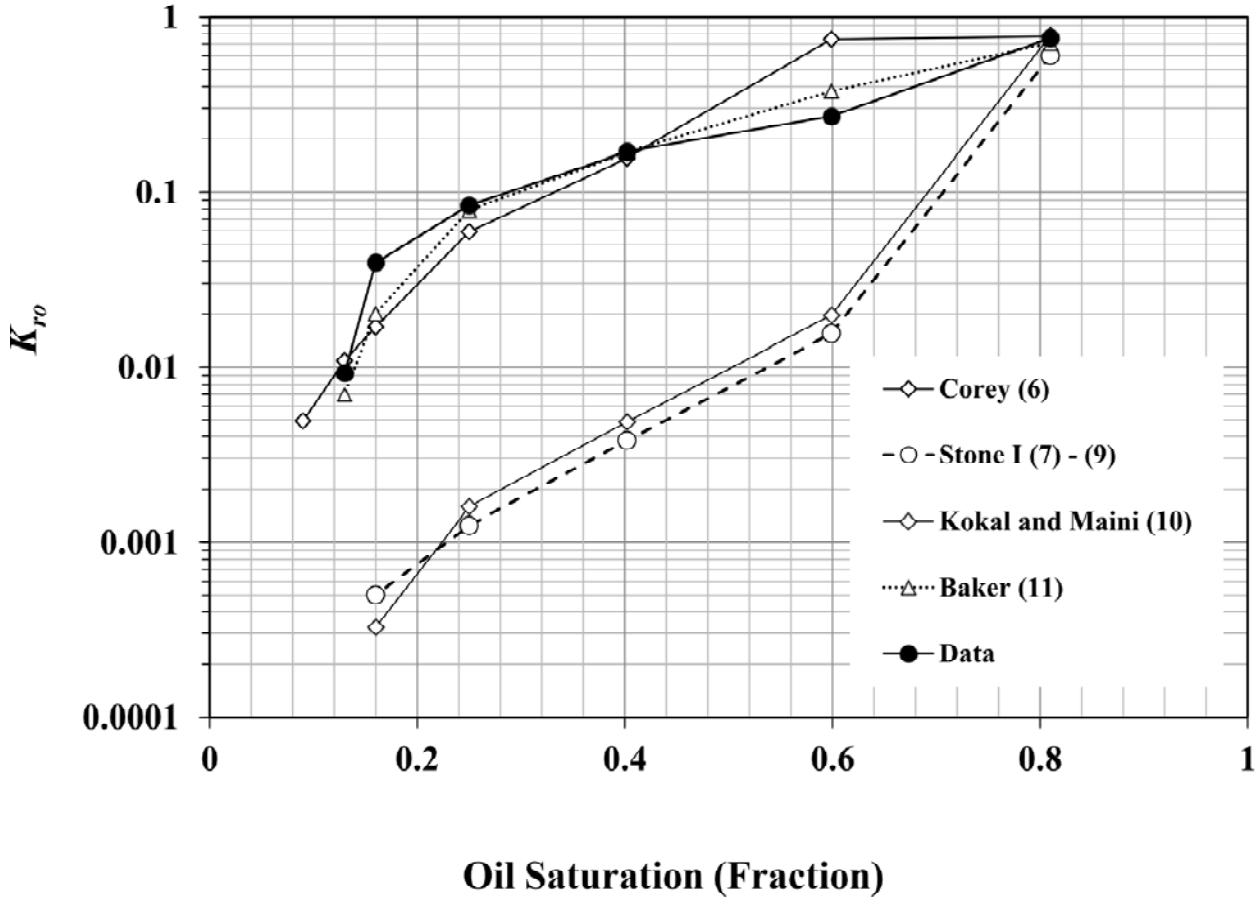

Fig. 12. Comparison between the Steady-State (SS) three-phase oil relative permeability data (K_{ro}) and the corresponding values obtained by applying the models illustrated in Section 2.6.

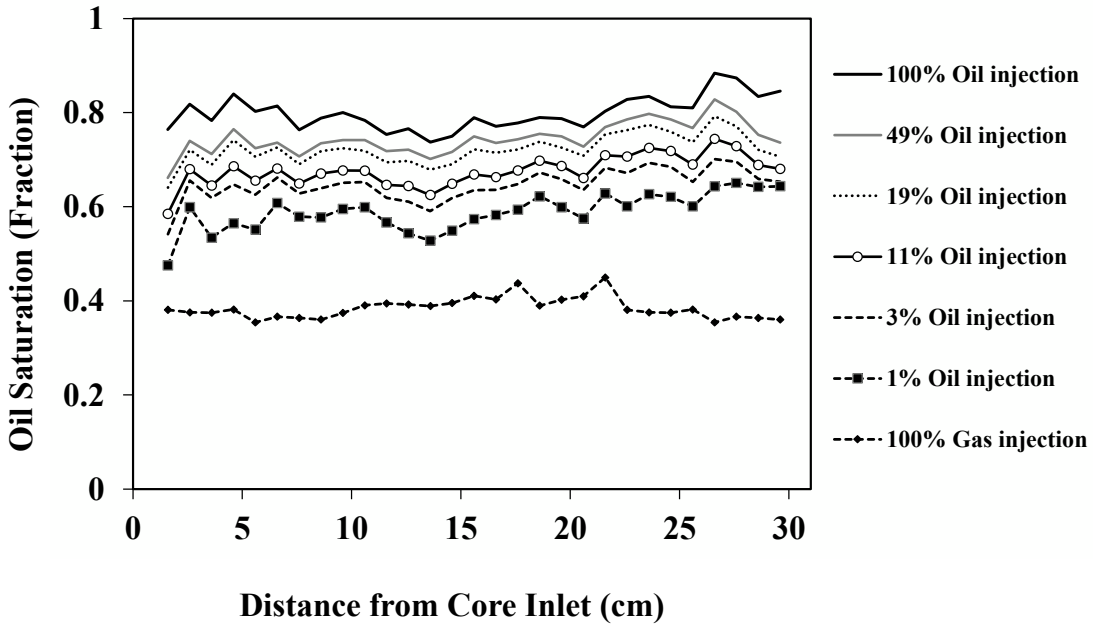

Fig. C1. In-situ Steady-State (SS) oil saturation profiles detected for the oil/gas system in the Sand-pack medium.

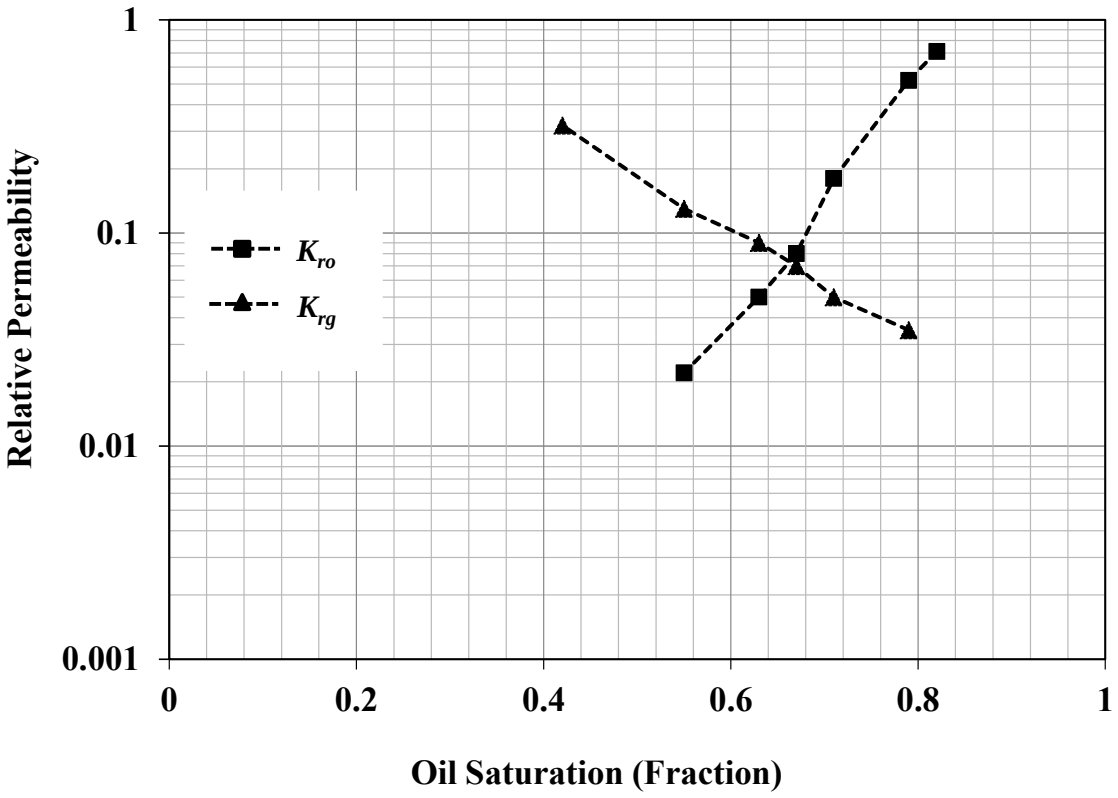

Fig. C2. In-situ Steady-State (SS) oil and gas relative permeabilities (respectively denoted as K_{ro} and K_{rg}) associated with the oil/gas system for the Sand-pack medium.

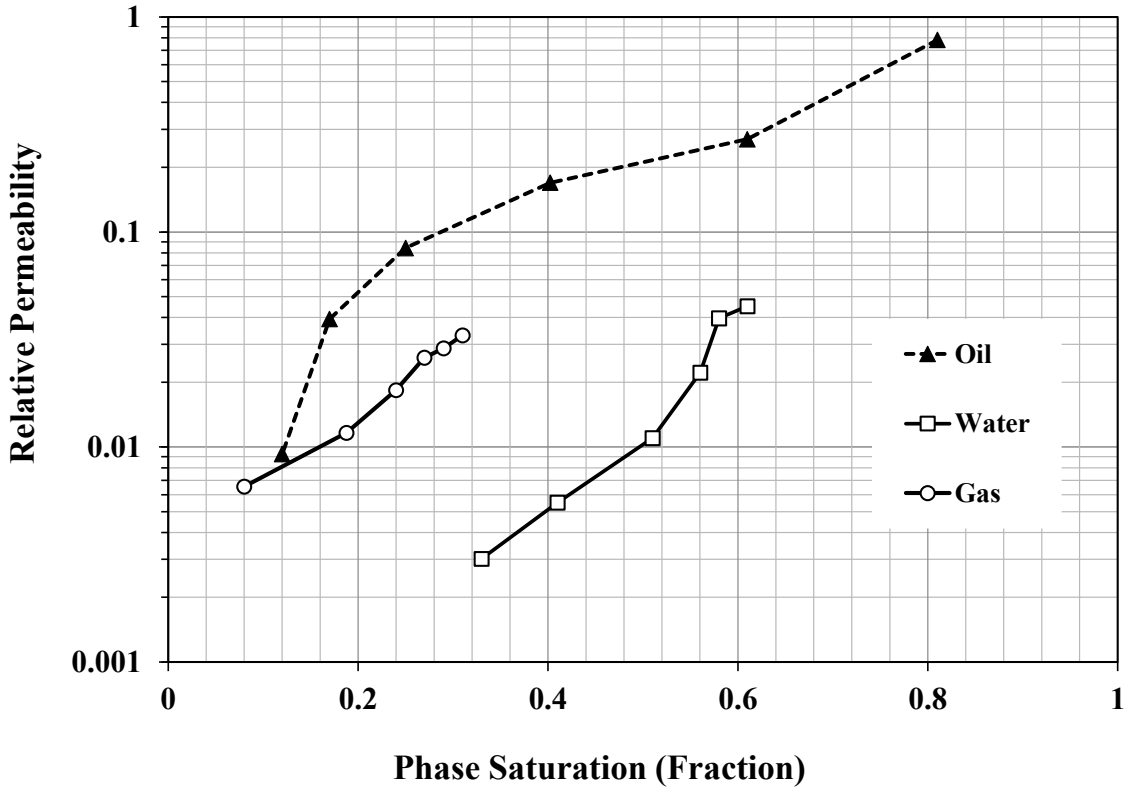

Fig. C3. Relative permeability to water, oil and gas as a function of the corresponding fluid saturation level.

Table 1. Physical properties of the tested core samples and fluids.

	Sand-pack	Berea	
		Soltrol	OB-12
Oil viscosity [cP]	1.74	1.74	25
Water viscosity [cP]	0.97	1.03	
Gas viscosity [cP]	0.018	____	
Porosity [%]	37	17	
Water absolute permeability [mD]	2900	30	
Permeability of oil at S_{wi} [mD]	2500	25	

Table 2. Values of the sum of squared deviations (12) associated with the oil relative permeability models illustrated in Section 2.6.

Models	$\sum DEV$ (12)
Corey (6)	0.05
Stone I (7) - (9)	0.12
Kokal and Maini (10)	0.09
Baker (11)	0.013